

Published in final edited form as:

*Biochemistry*. 2017 April 25; 56(16): 2197–2208. doi:10.1021/acs.biochem.7b00002.

# Structural Changes in an Anion Channelrhodopsin: Formation of the K and L Intermediates at 80 K

**Adrian Yi**[†], **Hai Li**[‡], **Natalia Mamaeva**[†], **Roberto E. Fernandez De Cordoba**[†], **Johan Lugtenburg**[§], **Willem J. DeGrip**[§], **John L. Spudich**[‡], and **Kenneth J. Rothschild**[*,†]

[†]Molecular Biophysics Laboratory, Photonics Center, and Department of Physics, Boston University, Boston, Massachusetts 02215, United States [‡]Center for Membrane Biology, Department of Biochemistry and Molecular Biology, The University of Texas Health Science Center at Houston, McGovern Medical School, Houston, Texas 77030, United States [§]Department of Biophysical Organic Chemistry, Leiden Institute of Chemistry, Leiden University, 2300 AR Leiden, The Netherlands

## Abstract

A recently discovered natural family of light-gated anion channelrhodopsins (ACRs) from cryptophyte algae provides an effective means of optogenetically silencing neurons. The most extensively studied ACR is from *Guillardia theta* (*Gt*ACR1). Earlier studies of *Gt*ACR1 have established a correlation between formation of a blue-shifted L-like intermediate and the anion channel "open" state. To study structural changes of *Gt*ACR1 in the K and L intermediates of the photocycle, a combination of low-temperature Fourier transform infrared (FTIR) and ultraviolet–visible absorption difference spectroscopy was used along with stable-isotope retinal labeling and site-directed mutagenesis. In contrast to bacteriorhodopsin (BR) and other microbial rhodopsins, which form only a stable red-shifted K intermediate at 80 K, *Gt*ACR1 forms both stable K and L-like intermediates. Evidence includes the appearance of positive ethylenic and fingerprint vibrational bands characteristic of the L intermediate as well as a positive visible absorption band near 485 nm. FTIR difference bands in the carboxylic acid C=O stretching region indicate that several Asp/Glu residues undergo hydrogen bonding changes at 80 K. The Glu68 → Gln and Ser97 → Glu substitutions, residues located close to the retinylidene Schiff base, altered the K:L

[*]**Corresponding Author:** Department of Physics, Boston University, 590 Commonwealth Ave., Boston, MA 02215. E-mail: kjr@bu.edu.

**Supporting Information**

The Supporting Information is available free of charge on the ACS Publications website at DOI: 10.1021/acs.bio-chem.7b00002. RRS data of *Gt*ACR1 regenerated with isotope labels (Figure S1), comparison of first-push FTIR difference spectra recorded using 530 and 455 nm illumination (Figure S2), FTIR difference spectra of *Gt*ACR1 recorded different times after illumination (Figure S3), exponential fitted kinetic plots of the intensity decay of the K intermediate and formation of the L intermediate at 170 K (Figure S4), two-dimensional folding pattern predicted for sequence of *Gt*ACR1 (Figure S5), low-temperature UV–visible absorption and difference spectra for *Gt*ACR1 mutant E68Q (Figure S6), and low-temperature UV–visible absorption and difference spectra for *Gt*CR1 mutant S97E (Figure S7) (PDF)

**ORCID**

Adrian Yi: 0000-0001-9067-724X
Willem J. DeGrip: 0000-0001-7637-4920
Kenneth J. Rothschild: 0000-0002-2847-6671

**Notes**

The authors declare no competing financial interest.

ratio and several of the FTIR bands in the carboxylic acid region. In the case of the Ser97 → Glu substitution, a significant red-shift of the absorption wavelength of the K and L intermediates occurs. Sequence comparisons suggest that L formation in *Gt*ACR1 at 80 K is due in part to the substitution of the highly conserved Leu or Ile at position 93 in helix 3 (BR sequence) with the homologous Met105 in *Gt*ACR1.

## Graphical abstract

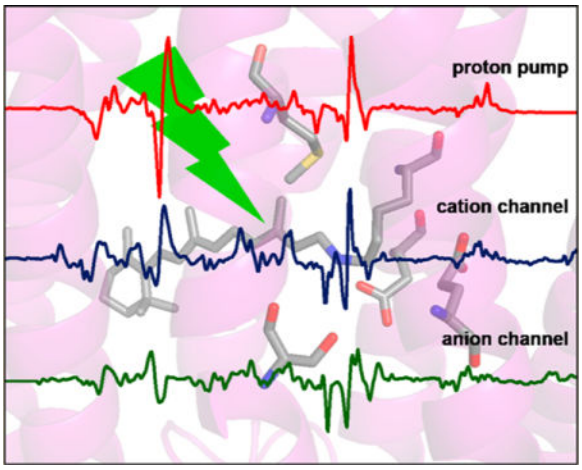


A new type of channelrhodopsin (ChR) has recently been discovered in cryptophyte algae termed anion channelrhodopsins (ACRs).[1] Unlike the more extensively studied cation channelrhodopsins (CCRs) from the phylogenetically distinct green chlorophyte algae, ACRs are exclusively anion selective and exhibit the highest conductance among ChRs thus far observed.[1,2] Importantly, ACRs provide an unprecedented effective means for low-light inhibition of neuronal and cardiomyocyte activity.[3] Silencing occurs because of light-induced anion channel opening that causes an influx of $Cl^-$ and subsequent hyperpolarization. In comparison to outwardly directed proton pumps such as archaerhodopsin-3 (AR3) or inwardly directed anion pumps such as halorhodopsins (HRs), both of which transport one ion for each photocycle,[4] ACRs require as little as 1/1000th of the light intensity necessary to achieve neuronal silencing.[1] ACRs also provide an opportunity to study the molecular basis for anion permeation and selectivity in seven-helix TM proteins.

An important goal is to understand the difference in molecular mechanisms that distinguish ACRs from CCRs and microbial rhodopsins in general. Recent studies of the light-induced photocurrent and photochemical reaction cycle of an ACR from *Guillardia theta* (designated *Gt*ACR1) reveal several distinct differences.[5,6] Most importantly, in 6 ns laser flash photolysis measurements, the Schiff base-deprotonated M intermediate occurs much later in ACRs than in any other microbial rhodopsins, including CCRs. The formation of a blue-shifted L-like intermediate (which may be in rapid equilibrium with pre-M red-shifted intermediate(s)) in the *Gt*ACR1 photocycle is correlated with the anion conducting “open” state of the channel while decay of the L intermediate (and formation of an M intermediate) with channel closing.[5,6] This is an unusual feature of ACRs because the “activated state” of

most microbial rhodopsins, such as signaling states of sensory rhodopsins, is associated with M formation and not the earlier K or L intermediates. For example, in the case of CCRs, the open channel state occurs after formation of an M-like intermediate often designated $P_2^{3807}$ and subsequent red-shifted (N/O) intermediates.[8,9]

To study the structural and protonation changes that occur in *Gt*ACR1 upon formation of the K and L intermediates, we performed low-temperature FTIR and ultraviolet–visible (UV–vis) difference spectroscopy on *Gt*ACR1 purified from a yeast (*Pichia pastoris*) expression system and reconstituted into a model lipid bilayer composed of *Escherichia coli* polar lipids (EPCLs). Several techniques were used to assign infrared vibrational bands, including stable-isotope retinal labeling, hydrogen/deuterium exchange, and site-directed mutagenesis. A surprising finding is that unlike most microbial rhodopsins, which form a stable K-like intermediate at 80 K, *Gt*ACR1 also forms a stable L-like intermediate. Sequence comparisons of ACRs with CCRs and microbial rhodopsins in general suggest that the substitution of a methionine for leucine or isoleucine at position 93 in CCRs (BR sequence) weakens steric interaction with the retinal 13-methyl group that at low temperatures blocks the relaxation of the retinylidene chromophore to form L. FTIR difference bands appearing in the carboxylic acid C=O stretch region at 80 K indicate that L formation involves hydrogen bonding changes of several Asp and/or Glu groups. The Glu68 → Gln and Ser97 → Glu substitutions, residues located close to the retinylidene Schiff base (SB), alter the ratio K:L produced at 80 K in addition to hydrogen bonding changes of Asp/Glu residues. In the case of the Ser97 → Glu substitution at neutral pH, a red-shift of the unphotolyzed state as well as the K and L states occurs compared relative to WT absorption. This indicates that the environment near the Schiff base becomes significantly altered and possibility less polar despite the addition of a carboxylic group.

## MATERIALS AND METHODS

### Expression, Purification, and Reconstitution of *Gt*ACR1

The 7TM domain of *Gt*ACR1 was expressed from *P. pastoris*,[1] purified, and reconstituted using a procedure described previously.[10] Purification was performed on a Ni-NTA agarose column (Qiagen, Hilden, Germany) after solubilization by incubation overnight in 3% *N*-octyl D-glucopyranoside (OG). For reconstitution, *E. coli* polar lipids (ECPL) (Avanti Polar Lipids, Alabaster, AL) were used at a 1:10 (w/w) ratio (*Gt*ACR1:ECPL). The final buffer used for storage of the membranes at 5 °C consisted of 5 mM $K_2HPO_4$ and 100 mM NaCl (pH 7.3). All mutants were generated using a similar procedure as described above (see also refs [5] and [10]).

### Chromophore Substitution with Isotope-Labeled all-*trans*-Retinal and Resonance Raman Measurements

The substitution of the native all-*trans*-retinal chromophore of *Gt*ACR1 with all-*trans*-[15-$^{13}$C,15-$^{2}$H]retinal and all-*trans*-[14,15-$^{2}H_2$]retinal followed similar procedures described previously for *Ca*ChR1.[11] Reconstituted *Gt*ACR1 membranes were suspended in 100 mM hydroxylamine buffer with 300 mM NaCl and 20 mM HEPES (pH 7) and exposed to 530 nm light-emitting diode (LED) illumination (5 mW/cm$^2$) for 40 min. Bleaching was

monitored by UV–visible spectroscopy using a Cary 6000 spectrometer (Agilent Technologies, Inc., Santa Clara, CA). After >95% conversion of the retinal chromophore to retinal oxime, the sample was pelleted using a SCILOGEX D3024 centrifuge spun at 21000*g* for 3 min and resuspended in wash buffer [300 mM NaCl and 20 mM HEPES (pH 7)]. This was repeated at least three times to remove unreacted/excess hydroxylamine and free retinal oxime. A 2-fold stoichiometric excess of the isotope-labeled retinal was then added as a 2 mM EtOH solution. The incorporation of the isotope-labeled retinal was verified by resonance Raman spectroscopy (RRS) using a Renishaw inVia confocal Raman microscope with 785-nm laser excitation similar to measurements previously reported.[10]

## Low-Temperature FTIR Difference Spectroscopy

Low-temperature FTIR difference measurements were performed using procedures similar to those previously reported for *Ca*ChR1.[11,12] A *Gt*ACR1/EPCL membrane sample containing approximately 50 μg of the protein was resuspended in 50 μL of buffer [50 mM NaCl and 5 mM HEPES (pH 7)] and deposited on a 17 mm diameter $BaF_2$ window. The sample was slowly dried in a drybox and then rehydrated through the vapor phase with a small drop (~0.5 μL) of $H_2O$ or $D_2O$ and sealed in a sample cell with another $BaF_2$ window. The cell was mounted in a liquid nitrogen cryostat (Oxford Instruments, OptistatDN). Measurements at different temperatures ranging from 80 to 270 K were performed by first cooling the sample from room temperature in the dark to avoid trapping of photointermediates. Once the sample reached the desired temperature, it was allowed to equilibrate in the dark for at least 30 min.

All spectra were recorded using a Bio-Rad FTS-60A FTIR spectrometer (Agilent Technologies, Inc.) equipped with a liquid nitrogen-cooled HgCdTe detector. Each acquired spectrum consisted of 200 scans (approximately 1 min of total acquisition time) recorded at 4 $cm^{-1}$ resolution. “First-push” difference spectra consisted of a spectrum recorded immediately before illumination (spectrum 1) subtracted from a spectrum recorded during illumination (spectrum 2) and termed “2–1” difference spectra. The light is then turned off, and 11 additional spectra are recorded (i.e., spectra 3–13) that are termed “decay” spectra and corresponding differences such as “3–1”, “4–1”, etc. Note that as the first-push and decay spectra were recorded at a specific temperature, samples were warmed to room temperature and allowed to rest in dark for at least 15 min before additional spectra were recorded at the same or different temperatures.

Difference spectra were also recorded at 80 K using photoreversal methods to measure multiple cycles of differences, which are subsequently averaged. In this case, individual spectra were recorded using the same FTIR acquisition parameters described above. A photoreversal cycle of four successively recorded spectra consisted of the following sample illumination conditions: (1) dark, (2) illumination with a 530 or 455 nm light (all LED illumination and LED control systems from Thorlabs, Inc., Newton, NJ), (3) dark, and (4) illumination with a 590 nm LED. This cycle was repeated at least 30 times, and the corresponding difference spectra (e.g., 2–1, 3–1, and 4–3) were calculated.

### Low-Temperature UV–Visible Absorption Difference Spectroscopy

Almost identical methods as described above for the FTIR difference first-push measurements were used to record low-temperature UV–visible difference spectra of *Gt*ACR1 (see also earlier UV–visible absorption studies of BR films[13]). Samples were prepared on $BaF_2$ windows as described above and loaded into the same liquid nitrogen cryostat except it was mounted in the sample compartment of a Cary6000 UV–visible absorption spectrometer. Spectra were acquired from 350 to 800 nm using a 0.1 s averaging time with 1 nm steps; each spectrum took slightly less than 1 min to acquire. Samples were cooled in the dark from room temperature and equilibrated at the desired temperature as described above. Three successive spectra were initially acquired, each starting 1 min apart, before the sample was illuminated with 530 nm light for 1 min. Immediately following the illumination, 30 or 120 successive spectra were acquired, each starting 1 min apart. The average of the three preillumination spectra is termed “pre-LED”, and the postillumination spectra are designated by the number of minutes after the illumination, with the first spectrum starting at “1”. The absolute absorbance spectra of *Gt*ACR1 films included contributions from the $BaF_2$ windows whose absorption changes as a function of temperature and contributes to the absorption at wavelengths of <400 nm. Individual difference spectra were baseline-corrected separately to account for the baseline drifts that occur throughout the experiment. The difference spectra were smoothed using five-point symmetric moving average, and then they were baseline-corrected using a combination of Tyndall and Rayleigh scattering terms and an additional linear term for the regions of spectra below 400 nm and above 700 nm.

## RESULTS

### Low-Temperature FTIR Difference Spectroscopy

**Ethylenic Region—**First-push “2–1” FTIR difference spectra of *Gt*ACR1 membranes recorded at 80 and 170 K are shown in Figure 1. These difference spectra reflect structural changes that occur in the protein and retinylidene chromophore during 530 nm illumination (e.g., photostationary state). Negative bands reflect vibrational modes arising from the unphotolyzed *Gt*ACR1 and positive bands those arising from the photo-products produced during illumination. To demonstrate the high reproducibility of even very small bands in these spectra, we show two independent measurements taken at each temperature (Figure 1). Overall, these difference spectra provide information about the progression of light-induced conformational changes that occur under these conditions during the early *Gt*ACR1 photocycle.

At 80 K, there are several unusual features of the *Gt*ACR1 FTIR difference spectrum compared to those of most other microbial rhodopsins, including BR and *Ca*ChR1 (Figure 2). As discussed below, several of these features are consistent with formation of an L-like intermediate at 80 K. First, the difference spectra in the ethylenic C=C stretch region (1500–1600 $cm^{-1}$) do not display the strong ethylenic “marker” band indicative of the formation of a red-shifted K-like photo-intermediate. The higher-frequency negative band normally corresponds to the depletion of the unphotolyzed state, while the positive lower-frequency bands correspond to the formation of the red-shifted K intermediate. For example, in the

case of BR and *Ca*ChR1 (Figure 2), a pair of strong negative/positive bands appears at 1530/1514 and 1535/1522 $cm^{-1}$, respectively. The downshift in ethylenic frequency ($\nu_{C=C}$) upon formation of K is expected due to the red-shift and the well-known inverse linear relationship between $\lambda_{max}$ and $\nu_{C=C}$.[14–16]

In the case of *Gt*ACR1, a strong negative band appears at 1530 $cm^{-1}$ (Figures 1 and 2), in agreement with near-IR resonance Raman measurements[10] (Figure S1). However, only a weak positive band appears at a lower frequency near 1506 $cm^{-1}$ in the first-push differences (Figure 1) and 1514 $cm^{-1}$ in the averaged photoreversal differences (Figure 2). In contrast, a much stronger positive band appears near 1545 $cm^{-1}$. On the basis of the inverse linear relationship between $\lambda_{max}$ and $\nu_{C=C}$,[14–16] this corresponds to a photoproduct with a $\lambda_{max}$ near 485 nm, in the range of the $\lambda_{max}$ of the *Gt*ACR1 L-like intermediate deduced from global fitting of the transient visible absorption spectra measured at room temperature.[5]

Because the amide II mode of $\alpha$-helices can also give rise to bands near 1545 $cm^{-1}$,[17] we measured *Gt*ACR1 regenerated with isotopically labeled all-*trans*-retinal at the [15-$^2$H, 15-$^{13}$C] and [14,15-$^2H_2$] positions. These isotope labels are expected to decrease the ethylenic frequency ($\nu_{C=C}$) based on earlier FTIR difference studies of BR and *Ca*ChR1.[11] As seen in Figure 3, the [15-$^2$H,15-$^{13}$C]- and [14,15-$^2H_2$]retinal substitutions cause the 1530 $cm^{-1}$ negative band to downshift by 10 and 18 $cm^{-1}$, respectively. Importantly, this agrees with shifts observed from near-IR resonance Raman measurements that are expected to be sensitive to predominantly the chromophore vibrational modes (Figure S1). In addition, the 1545 $cm^{-1}$ positive band downshifts 8 and 10 $cm^{-1}$ for the [15-$^2$H,15-$^{13}$C]- and [14,15-$^2H_2$]retinal labels, respectively (Figure 3). The different extent of isotope band shifts for the 1530 $cm^{-1}$ negative and 1545 $cm^{-1}$ positive bands most likely reflects the different extent of mode coupling expected for all-*trans* and 13-*cis* isomeric states of the retinylidene chromophore.[18,19] Overall, these results indicate that at 80 K the 1545 $cm^{-1}$ band arises from a retinal ethylenic mode of an L-like intermediate and not from the amide II mode of the protein. In addition, the absence of a strong positive band corresponding to the K intermediate may indicate a level of K production much lower than that normally observed under these conditions. The possibility also exists that considerable positive intensity of the K intermediate ethylenic band is canceled by the negative band at 1530 $cm^{-1}$, which could reflect less separation between the unphotolyzed and photolyzed visible absorption ($\lambda_{max}$).

We also considered the possibility that an L-like species observed at 80 K arises from photoreaction of a stable K intermediate formed at 80 K. However, almost identical results are obtained using 455 nm illumination (Figure S2) even though the K intermediate is expected to absorb less light of this wavelength compared to 530 nm light. This result may indicate the K and L intermediates produced at 80 K exist in equilibrium, similar to the conclusion from room-temperature visible absorption measurements.[5] In addition, successive first-push decay difference spectra recorded at approximately 1 min intervals after the exciting light is turned off (Figure S3) reveal very little change compared to the initial “2–1” difference spectrum. This result eliminates the possibility that an L-like photoproduct corresponding to the 1545 $cm^{-1}$ band is a transient species at 80 K that accumulates during illumination.

**Fingerprint Region—**A second unusual feature of the *Gt*ACR1 80 K difference spectra is found in the fingerprint region (1100–1250 $cm^{-1}$) (Figures 1 and 2). Bands in this region arise from the mixed C–C stretching modes of the retinal polyene chain. Such band frequencies ($\nu_{C-C}$) are highly sensitive to the retinal configuration.[18,19] In the case of *Gt*ACR1, the negative bands in this region appear near 1200 and 1161 $cm^{-1}$ similar to the $\nu_{C-C}$ frequencies found for BR and *Ca*ChR1 (Figure 2). This supports the earlier conclusion based on near-IR resonance Raman spectroscopy (RRS) that the unphotolyzed state of *Gt*ACR1 has a predominantly all-*trans*-retinal configuration.[20]

*Gt*ACR1 also displays a strong positive band in the fingerprint region at 1182 $cm^{-1}$ along with an additional shoulder at 1192 $cm^{-1}$ (Figures 1 and 2). However, the 1182 $cm^{-1}$ band is at an unusually low frequency for a K-like intermediate. For example, *Ca*ChR1 and BR display the most intense positive band in this region near 1195 $cm^{-1}$ (Figure 2) as do most other microbial rhodopsins. Another unusual feature compared to BR is the appearance of a positive 1146 $cm^{-1}$ band. This band is close to the frequency of a positive band at 1154 $cm^{-1}$ appearing in the BR → L difference spectrum[21] and assigned to the $C_{14}$–$C_{15}$ stretch mode on the basis of isotope labeling.[22] In the case of *Gt*ACR1, the effect of the [15-$^{2}$H, 15-$^{13}$C] and [14,15-$^{2}H_2$] retinylidene isotope labels (Figure 3) is also consistent with the assignment of this band to the $C_{14}$–$C_{15}$ stretch mode (Figure 3).

**Schiff Base and Amide I Region—**Bands due to both the Schiff base (SB) C=N stretching mode and the amide I mode of the protein peptide backbone can appear in the 1600–1700 $cm^{-1}$ region.[17,23] In the case of *Gt*ACR1, the strongest band in this region is located at (−)1634 $cm^{-1}$ (Figures 1 and 2), close to the frequency assigned to the C=N SB mode in the RRS of *Gt*ACR1.[10] Confirming this assignment, we found the (−)1634 $cm^{-1}$ band downshifts to 1622 $cm^{-1}$ upon H/D exchange (Figure 4) because of deuteration of the SB, again in agreement with the RRS results.[10] Much smaller bands also appear in this region at (+)1676, (−)1666, (−)1661, and (−)1651 $cm^{-1}$, which are not affected by isotope labeling or H/D exchange (Figures 3 and 4). Thus, we conclude that only small protein structural changes involving the peptide backbone of *Gt*ACR1 occur at 80 K.

**Carboxylic Acid C=O Stretch Region—**Bands in the 1700–1800 $cm^{-1}$ region arise mainly from changes in the C=O stretching mode of carboxylic acid groups reflecting protonation and/or hydrogen bond changes of Asp/Glu residues.[24–26] Several weak but highly reproducible bands are detected at 80 K, near (+)1748, (−)1741, (+)1734, (−)1728, (+)1722, (−)1705, and (+)1697 $cm^{-1}$ (Figure 5). At 170 K, all of these bands are still detected; however, the intensities of several increase significantly [(+)1748 and (−)1741 $cm^{-1}$], while others appear to maintain their intensity at (+)1734, (−)1728, and (+)1697 $cm^{-1}$. Two new bands also appear at (+)1724 and (−)1709 $cm^{-1}$ (Figure 5), which grow more intense at even higher temperatures (A. Yi et al., unpublished data) along with the (+)1748 and (−)1741 $cm^{-1}$ bands. Although it is not possible from these data to clearly separate out the bands due to the K and L intermediates, it is likely the (+)1724 and (−)1709 $cm^{-1}$ bands reflect changes occurring in the L intermediate at 170 K but not 80 K (see Discussion).

### Low-Temperature UV–Visible Absorption Difference Spectroscopy

UV–visible absorption spectra of *Gt*ACR1 were recorded at 80 and 170 K on hydrated films under conditions almost identical to those used for the FTIR measurements. A major band appears at 517 nm with a shoulder at 467 nm (Figure 6A), close to the wavelengths of bands measured at room temperature from suspensions of the reconstituted *Gt*ACR1 membrane (see the Supporting Information of ref [10]).

Difference spectra, which reflect changes in the UV–visible absorption immediately before and at specific times after 530 nm illumination (see Materials and Methods), reveal no significant spectral change over a 30 min period. This indicates that the photocycle intermediates produced at this temperature are stable (Figure 6B). A positive peak appears at 565 nm corresponding to the production of a K-like red-shifted intermediate, while two negative bands appear at 510 and 467 nm, which are close to the wavelengths of the absorption maxima of the unphotolyzed *Gt*ACR1 (Figure 6A). However, the ratios of the negative band intensities at 467 and 510 nm are similar despite the much smaller absorbance of the 467 nm band relative to that of the 517 nm band in the absolute absorption (Figure 6A).

One explanation for this effect is that at 80 K an L-like blue-shifted photoproduct is produced in addition to K. This L-like intermediate is expected to produce positive intensity near 485 nm and thus could act to cancel negative intensity due to depletion of the unphotolyzed state. To test this explanation, we measured the difference spectra of *Gt*ACR1 at 170 K, where in analogy to BR the K intermediate is not expected to be stable.[27,28] In fact, a K → L decay at this temperature is directly inferred from the difference spectrum (Figure 6C), where the intensity of the positive band at 570 nm reflecting the level of the K intermediate slowly decreases while the intensity of the positive feature near 485 nm increases. Postillumination differences (e.g., changes in absorption immediately after illumination subtracted from those at later times) clearly show the formation of a broad band centered near 485 nm reflecting accumulation of the L intermediate, concomitant with a decrease in the intensity of a negative band near 570 nm indicative of a decay of the K intermediate (Figure 6D). Note that the L intermediate produced during K decay may consist of several different species as indicated by the apparent subcomponent bands.

The K decay kinetics were also curve fit in the range of 535–595 nm with a double exponential revealing two time constants for the K → L transition of approximately 5 and 50 min (Figure S4). L rise kinetics fit over 455–475 and 500–520 nm ranges also gave similar but not identical kinetics of approximately 4 and 40 min (data not shown). We thus conclude on the basis of both the low-temperature FTIR and UV–visible absorption measurements that at 80 K, photo-illumination of *Gt*ACR1 results in the production of both K and L-like intermediates that are stable (e.g., do not decay). At 170 K, the K intermediate is no longer stable and slowly decays to produce the L intermediate.

**Effects of Substitutions Located near the Schiff Base. Glu68 → Gln—**Glu68, located on helix 2 of *Gt*ACR1 (Figure S5) (the homologue of Glu90 in *Cr*ChR2, the cation channel from *Chlamydomonas reinhardtii*), is predicted to be close to the Schiff base on the basis of the X-ray crystallographic structure of the ChR chimera (termed the C1–C2

chimera)[29] (see Figure 10B). Previous studies have shown that the Glu68 → Gln substitution (E68Q) has significant effects on the channel gating mechanism[6] but only a weak effect on the visible absorption.[5,10] In agreement, at 80 K, UV–visible absorption of E68Q is very similar to that of WT (Figure S6A). However, the difference spectrum compared to that of WT (Figure 7 and Figure S6B) displays an increased negative intensity and a downshift in the wavelength of the major negative band (from 510 to 503 nm). Both effects can be explained if less L intermediate in E68Q is produced than in WT (thereby producing less cancelation of the negative band due to depletion of the unphotolyzed species). Similar to WT, E68Q still exhibits a stable K and L at 80 K and a K → L decay at 170 K with kinetics similar to those of WT (Figures S4 and S6B–D).

The 3–1 first-push FTIR difference spectrum of E68Q also indicates that less L is produced and more K intermediate is produced at 80 K after the light is turned off (Figure 8). The intensity of the negative ethylenic band at (−)1530 $cm^{-1}$ is lower than that of the WT ethylenic bands. This decrease in intensity can be explained by an increased level of cancellation of the negative 1530 $cm^{-1}$ band by a hidden positive K band near 1520 $cm^{-1}$. In addition, the most intense band in the fingerprint region is at 1190 $cm^{-1}$, which may be associated with the K intermediate (see above), while the peak at 1146 $cm^{-1}$ associated with the L intermediate is weaker than that of WT. In the 1700–1800 $cm^{-1}$ carboxylic acid C=O stretch region (Figure 9), bands located at (+)1734, (−)1728, (+)1722, and (−)1705 $cm^{-1}$ in WT are all absent in E68Q while a new set of bands appears at (−)1693 and (+)1686 $cm^{-1}$. These later bands might arise from the C=O stretch of the substituted Gln residue similar to assignment of Gln residues in proteorhodopsin in this region.[30] At 170 K, the magnitudes of several of the bands in this region in WT increase [(+)1748, (−)1742, (+)1724, and (−)1709 $cm^{-1}$] and may therefore be associated with L formation at higher temperatures. The most prominent effect of the E68Q mutation at this temperature is the disappearance of the (+)1724 and (−)1709 $cm^{-1}$ bands, which indicates that these bands may arise directly from the Glu68 residue.

**Ser97 → Glu—**Ser97, located on helix 3 (Figure S5), is the homologue of Asp85, the primary SB counterion and proton acceptor in BR. An earlier study of the Ser97 → Glu substitution (S97E) using RRS found that at pH 7 the ethylenic $\nu_{C=C}$ undergoes an ~4 $cm^{-1}$ downshift that would correspond to an ~16 nm red-shift in the visible $\lambda_{max}$.[10] This indicates that at neutral pH the substituted Glu97 carboxylic acid group exists in a neutral form, or else one would expect the substitution to cause a substantial blue-shift. This red-shifting effect is analogous to formation of the BR blue membrane, where protonation of the Asp85 counterion at low pH causes a red-shift of the visible absorbance and a corresponding downshift in $\nu_{C=C}$.[31] However, in the case of *Gt*ACR1 S97E, the p$K_a$ of the carboxylic acid group of Glu97 appears to be much higher than that of Asp85 in BR.

Although the 80 K visible absorption of S97E did not show a red-shift in the wavelength maximum and indeed appears to be blue-shifted to 512 nm (Figure S7A), the initial difference spectrum and subsequent spectra reveal a shoulder at a higher wavelength near 540 nm (Figure S7B). This may indicate that the S97E mutant under these conditions comprises a mixture of two different species that are blue-shifted and red-shifted relative to WT. In fact, RRS studies reveal at pH >7 a mixture of red- and blue-shifted species exist

corresponding to ethylenic bands at 1528 and 1545 $cm^{-1}$ (note WT is at 1530 $cm^{-1}$). It was predicted that the intensity of the blue-shifted species that increases at higher pH corresponds to deprotonation of Glu97.[10] The S97E UV–visible difference spectra at 80 K also reveal that the K intermediate formed at this temperature is significantly red-shifted as indicated by the upshift in the positive band by 25 nm compared to WT (Figure S7B). At 170 K, the K intermediate still appears to be significantly red-shifted compared to WT by the same extent (Figure S7C). In addition, the L intermediate formed from decay of the K intermediate at this temperature is red-shifted (Figure S7D).

The FTIR difference spectrum of S97E (Figures 8 and 9) also supports many of the conclusions from low-temperature visible absorption measurements. The negative ethylenic band downshifts from 1530 to 1528 $cm^{-1}$, indicating the existence of a red-shifted species. This band is also more negative relative to WT potentially because of less overlap with a hidden positive K ethylenic, which has also downshifted, although we do not see a positive ethylenic corresponding to the K intermediate. The (+)1545 $cm^{-1}$ band in WT assigned to the L intermediate ethylenic is also downshifted to 1541 $cm^{-1}$, and its intensity is reduced, the latter effect potentially being caused by the lower level of L production. Interestingly, at 170 K, there is almost no accumulation of the L intermediate immediately after the light is turned off as indicated by the near disappearance of the 1545 $cm^{-1}$ band. This is in accord with the rapid L to M decay found at room temperature for the S97E mutant compared to WT based on flash-induced absorption changes.[5] One of the most unusual features of the FTIR difference spectrum is the appearance of a negative/positive pair of peaks near (−)1709/(+)1720 $cm^{-1}$ in the C=O stretch region (see Figure 9), which may reflect a hydrogen bonding change in the E97 carboxylic acid residue.

## DISCUSSION

Earlier studies of *Gt*ACR1 based on laser flash photocurrent measurement and transient visible absorption spectroscopy have established a correlation between anion channel opening and formation of the L intermediate and possibly pre-M red-shifted species with which the L intermediate is in rapid equilibrium.[5,6] This is an unusual feature because the “activated state” of microbial rhodopsins (e.g., the open-channel form of CCRs) normally occurs after transfer of a proton from the SB to an acceptor group during M formation (e.g., Asp85 in BR). However, in the case of *Gt*ACR1, the channel is open and the SB of L is still protonated similar to the case for other microbial rhodopsins as indicated by its visible absorption near 485 nm (see Results and ref [5]).

A key goal of this work is to investigate the molecular changes underlying the early steps in the *Gt*ACR1 photocycle and especially changes that occur upon K and L formation. Until now, only the structure of the unphotolyzed *Gt*ACR1 retinylidene chromophore has been characterized and found using RRS to exist in an all-*trans* conformation similar to light-adapted BR.[10] A similar conclusion was also reached on the basis of RRS for *Ca*ChR1 (a cation conducting channel from *Chlamydomonas augustae*).[20] Both of these ChRs do not exhibit light–dark adaptation.[5,10,20] In contrast, a heterogeneous chromophore configuration consisting of a mixture of all-*trans*- and 13-*cis*-retinal has been found to be present in *Ct*ChR2, which does undergo light–dark adaptation.[20,32,33] In general, ACRs similar to

CCRs exhibit diverse properties such as kinetics, conductance, and spectral sensitivity,[34] and thus, it is not possible to generalize about their chromophore and protein structures, even in the unphotolyzed state, without detailed examination of individual ChRs.

This work advances our understanding of *Gt*ACR1 by providing information about the structural changes that occur at low temperatures leading to formation of the K and L intermediates. Low-temperature spectroscopic studies have previously been extensively performed on a variety of microbial rhodopsins and provided important information. For example, the ability to trap or partially block the decay of photocycle intermediates offers a means to characterize their spectral properties for example by the application of resonance Raman, FTIR, UV–visible, and NMR.[35–39] In conjunction with the ability to crystallize some microbial rhodopsin such as BR, low temperatures provide a way to trap these proteins in pure or mixtures of different photointermediates that can be analyzed in parallel by both spectroscopy and X-ray crystallography.[40]

However, low-temperature spectroscopic studies may introduce changes relative to the room-temperature photocycle of microbial rhodopsins.[41] For this reason, time-resolved room-temperature spectroscopic studies performed under more physiological conditions are an important complement to low-temperature studies. For example, extensive time-resolved visible and FTIR difference studies have been performed on BR[42] and more recently *Ct*ChR2.[8,33,43–49] In one study, time-resolved FTIR and UV–vis difference spectroscopy combined with MSD calculation led to the proposal that a downward movement of Glu90 (homologue of Glu68 in *Gt*ACR1) causes helix 2 to tilt downward, thereby resulting in channel opening.[44]

Several key results of this study are discussed below.

## Substitution of a Met in ACRs at the Position of Conserved Leu93 (BR sequence) Might Allow the L Intermediate To Form at Lower Temperatures

The primary photoproduct of almost all microbial rhodopsins is a red-shifted K intermediate. In the case of BR, formation of K entails the light-induced all-*trans*, 15-*anti* to 13-*cis*, 15-*anti* isomerization of the retinylidene chromophore.[50] At room temperature, the K intermediate undergoes a rapid (~2 $\mu$s) thermal decay to a blue-shifted L intermediate with a more planar 13-*cis*, 15-*anti* configuration.[51–53] However, at 80 K, the K → L transition is normally blocked. Besides BR,[35,54] this block has been observed in prokaryotic sensory rhodopsins (SRI and SRII),[55,56] fungal *Neurospora* rhodopsin (NO),[15] *Anabaena* sensory rhodopsin from cyanobacteria (ASR),[57] and green- and blue-absorbing proteorhodopsin proton pumps from marine protobacteria (GPR and BPR, respectively),[14,30,58–63] archaerhodopsin-3 (AR3, also known as ARCH), a BR-like proton pump,[64,65] and channelrhodopsins (ChRs) from chlorophyte algae.[10–12,20] Even in the case of animal rhodopsins, which contain an 11-*cis*-retinylidene chromophore in the unphotolyzed rhodopsin state, the primary red-shifted bathorhodopsin photoproduct is blocked at 80 K from decaying to lumirhodopsin, the next step in the rhodopsin bleaching sequence.[66]

In contrast, this study indicates that both the K and L intermediates are formed at 80 K upon illumination of *Gt*ACR1. Evidence includes the appearance of bands in the FTIR spectrum

and the visible absorption difference spectra that are characteristic of the K and L intermediates (see Results). One possible explanation for this effect is that steric hindrance between the protein and retinal chromophore, which acts to block the K → L transition in most microbial rhodopsins, is reduced in the case of *Gt*ACR1.

In the case of BR, a major source of this steric hindrance is the well-known interaction between the 13-methyl group of retinal and the Leu93 located on helix 3.[67,68] On the basis of the X-ray structure of the C1–C2 chimera,[29] Ile170 (C1–C2 numbering) is in the proximity of the 13-methyl group (Figure 10B) and thus likely to play a similar role in blocking the K → L transition in CCRs. We suggest that replacement of the conserved Leu93 in BR and Leu/Ile in most other microbial rhodopsins with a methionine residue (Met105) in *Gt*ACR1 (see Figure 10A and Figure S5)[1] acts to lower the thermal barrier for the K → L transition at 80 K, thereby allowing the retinal to more easily relax into a more planar form characteristic of the L intermediate.[69] In support of this suggestion, the Leu93 → Met substitution in BR allows formation of the L intermediate at 80 K[21] similar to the case for *Gt*ACR1. Evidence includes results of low-temperature FTIR difference spectroscopy at 80 K where bands characteristic of the L intermediate appear to be similar to results described above for *Gt*ACR1. Similar effects were also found to occur for the Trp182 → Phe substitution, which is also expected to reduce steric hindrance in BR due to the proximity of Trp182 to the 13-methyl group.[21] However, in the case of *Gt*ACR1, this tryptophan residue is conserved and thus cannot be responsible for the difference between BR and *Gt*ACR1 with regard to L formation in the latter at 80 K. The presence of a Met residue at the Leu93 position in BR is not an absolute requirement for an ACR. Sequence alignments of ACR homologues show high conservation of Met, but an Ile or Leu residue is also observed at this position.[70]

It is not clear why a Leu to Met substitution would cause this effect because they have approximately the same average volume calculated from the surface area of the side chain.[71] One possibility is that the lower thermal barrier for the K → L transition in *Gt*ACR1 is due in part to an alteration in the arrangement of water molecules located near the SB when Met instead of Leu or Ile is present at homologous position 93 in BR. For example, an earlier study indicated that the Leu93 → Met substitution in BR causes substantial changes in the hydrogen bonding of one or more internal water molecules located near the SB.[21]

The importance of the residue present in position 93 is also supported by studies of proteorhodopsin (PR), a member of an extensive family of microbial rhodopsins found in marine proteobacteria distributed throughout the world's oceans.[72,73] Substituting the homologous residue from Leu105 with Gln switches the major properties of PRs from the green-absorbing GPRs to blue-absorbing BPRs.[74] FTIR studies of the primary transition of BRP and GPR demonstrated that one of the major effects of this substitution is to cause a rearrangement of internal waters located in the active site.[61] Further studies of mutants at this position in *Gt*ACR1 (e.g., M105L) as well as other microbial rhodopsins will be necessary to further test this hypothesis.

### Protein Changes Accompanying K and L Formation at Low Temperatures in *Gt*ACR1

FTIR difference measurements taken at 80 and 170 K reveal that only local protein structural changes occur in *Gt*ACR1 during formation of the K and L intermediates at these temperatures. For example, relatively small bands appear in the amide I region (excluding the SB C=N vibration assigned to the negative 1634 $cm^{-1}$ band) indicating that no large protein conformational changes occur under these conditions. However, much larger bands appear at higher temperatures in the amide I and II regions that may correspond to more global changes in the protein structure associated with the L intermediate and channel opening that are inhibited at lower temperatures (A. Yi et al., unpublished data).

A similar pattern is observed in the carboxylic C=O stretching region. At 80 K, only small bands are observed, consistent with a change in hydrogen bonding of several Asp/Glu carboxylic residues. At 170 K, the intensity of the pair of bands at (+)1748 and (−)1742 $cm^{-1}$ increases, while a new set of bands appear at (+)1724 and (−)1709 $cm^{-1}$. The intensity of both sets of bands continues to increase to 250 K (A. Yi et al., unpublished data). However, the (+)1724 and (−)1709 $cm^{-1}$ bands are abolished by the E68Q mutation, while the (+)1748 and (−)1741 $cm^{-1}$ bands are not. On this basis, we tentatively assign the (+)1724 and (−)1709 $cm^{-1}$ bands to changes in the hydrogen bonding of Glu68. Previously, Glu68, which is located close to the SB (Figure 10B), has been implicated as the proton acceptor for SB deprotonation during M formation.[6] We therefore suggest that the positive and negative bands at (+)1724 and (−)1709 $cm^{-1}$ may be associated with a repositioning and/or change in the environment of Glu68. This change could be associated with channel opening, which puts E68 in a position to act as the SB proton acceptor during channel closing.

### Effect of the Substitution of a Glu at Ser97 Causes a Red-Shift of the K and L Intermediates

It has previously been reported that the Ser97 → Glu substitution causes a redshift in the unphotolyzed state of *Gt*ACR1.[5,10] The current results show that a similar red-shift also occurs for the K and L intermediates. This indicates that the substituted Glu97 remains in a neutral state at pH 7 at least until production of the M intermediate (see also ref [6]), or else we would expect the negative charge on the carboxylate Glu97 side chain to cause a significant blue-shift. One possible explanation for the red-shifts observed in the unphotolyzed *Gt*ACR1 and the K and L intermediates is that the hydroxyl group of the Ser97 is more effective in providing an electronegative environment for the SB relative to the longer Glu97 even though the carboxylic group of Glu contains an additional electronegative oxygen. This might occur via the direct proximity of the serine hydroxyl or via one or more water molecules positioned near the SB.

## Supplementary Material

Refer to Web version on PubMed Central for supplementary material.

## Acknowledgments

We thank Sergey Mamaev for his advice and assistance with growth, purification, and expression of *Gt*ACR1.

**Funding**

This work was supported by National Science Foundation Grant CBET-1264434 to K.J.R. and National Institutes of Health Grant R01GM027750, a grant from the Hermann Eye Fund, and Endowed Chair AU-0009 from the Robert A. Welch Foundation to J.L.S.

## ABBREVIATIONS

| | |
|---|---|
| **ChRs** | channelrhodopsins |
| **ACR** | anion channelrhodopsin |
| **CCR** | cation channelrhodopsin |
| **RRS** | resonance Raman spectroscopy |
| **FTIR** | Fourier transform infrared |
| ***Gt*ACR1** | ACR from *G. theta* |
| ***Ca*ChR1** | channelrhodopsin-1 from *C. augustae* |
| ***Cr*ChR2** | channelrhodopsin-2 from *C. reinhardtii* |
| **BR** | bacteriorhodopsin |
| **HR** | halorhodopsin |
| **WT** | wild-type |
| **H/D** | hydrogen/deuterium |
| **SB** | protonated Schiff base |
| **C1–C2** | chimera of *Cr*ChR1 and *Cr*ChR2 |

## References

1. Govorunova EG, Sineshchekov OA, Janz R, Liu X, Spudich JL. Natural light-gated anion channels: A family of microbial rhodopsins for advanced optogenetics. Science. 2015; 349:647–650. [PubMed: 26113638]
2. Govorunova EG, Sineshchekov OA, Spudich JL. Proteomonas sulcata ACR1: A Fast Anion Channelrhodopsin. Photochem Photobiol. 2016; 92:257. [PubMed: 26686819]
3. Govorunova EG, Cunha SR, Sineshchekov OA, Spudich JL. Anion channelrhodopsins for inhibitory cardiac optogenetics. Sci Rep. 2016; 6:33530. [PubMed: 27628215]
4. Chow BY, Han X, Dobry AS, Qian X, Chuong AS, Li M, Henninger MA, Belfort GM, Lin Y, Monahan PE, Boyden ES. High-performance genetically targetable optical neural silencing by light-driven proton pumps. Nature. 2010; 463:98–102. [PubMed: 20054397]
5. Sineshchekov OA, Li H, Govorunova EG, Spudich JL. Photochemical reaction cycle transitions during anion channelrhodopsin gating. Proc Natl Acad Sci U S A. 2016; 113:E1993–2000. [PubMed: 27001860]
6. Sineshchekov OA, Govorunova EG, Li H, Spudich JL. Gating mechanisms of a natural anion channelrhodopsin. Proc Natl Acad Sci U S A. 2015; 112:14236–14241. [PubMed: 26578767]
7. Sineshchekov OA, Govorunova EG, Wang J, Li H, Spudich JL. Intramolecular proton transfer in channelrhodopsins. Biophys J. 2013; 104:807–817. [PubMed: 23442959]

8. Lorenz-Fonfria VA, Heberle J. Channelrhodopsin unchained: structure and mechanism of a light-gated cation channel. Biochim Biophys Acta, Bioenerg. 2014; 1837:626–642.
9. Schneider F, Grimm C, Hegemann P. Biophysics of Channelrhodopsin. Annu Rev Biophys. 2015; 44:167–186. [PubMed: 26098512]
10. Yi A, Mamaeva N, Li H, Spudich JL, Rothschild KJ. Resonance Raman Study of an Anion Channelrhodopsin: Effects of Mutations near the Retinylidene Schiff Base. Biochemistry. 2016; 55:2371–2380. [PubMed: 27039989]
11. Ogren JI, Yi A, Mamaev S, Li H, Lugtenburg J, DeGrip WJ, Spudich JL, Rothschild KJ. Comparison of the Structural Changes Occurring during the Primary Phototransition of Two Different Channelrhodopsins from Chlamydomonas Algae. Biochemistry. 2015; 54:377–388. [PubMed: 25469620]
12. Ogren JI, Yi A, Mamaev S, Li H, Spudich JL, Rothschild KJ. Proton transfers in a channelrhodopsin-1 studied by Fourier transform infrared (FTIR) difference spectroscopy and site-directed mutagenesis. J Biol Chem. 2015; 290:12719–12730. [PubMed: 25802337]
13. Ahl PL, Stern LJ, During D, Mogi T, Khorana HG, Rothschild KJ. Effects of amino acid substitutions in the F helix of bacteriorhodopsin. Low temperature ultraviolet/visible difference spectroscopy. J Biol Chem. 1988; 263:13594–13601. [PubMed: 3047127]
14. Bergo V, Amsden JJ, Spudich EN, Spudich JL, Rothschild KJ. Structural changes in the photoactive site of proteorhodopsin during the primary photoreaction. Biochemistry. 2004; 43:9075–9083. [PubMed: 15248764]
15. Bergo V, Spudich EN, Spudich JL, Rothschild KJ. A Fourier transform infrared study of Neurospora rhodopsin: similarities with archaeal rhodopsins. Photochem Photobiol. 2002; 76:341–349. [PubMed: 12403457]
16. Bergo V, Spudich EN, Spudich JL, Rothschild KJ. Conformational changes detected in a sensory rhodopsin II-transducer complex. J Biol Chem. 2003; 278:36556–36562. [PubMed: 12821665]
17. Parker, FS. Applications of infrared, Raman and resonance Raman spectroscopy in biochemistry. Plenum Press; New York: 1983.
18. Smith SO, Pardoen JA, Lugtenburg J, Mathies RA. Vibrational analysis of the 13-cis-retinal chromophore in dark-adapted bacteriorhodopsin. J Phys Chem. 1987; 91:804–819.
19. Smith SO, Braiman MS, Myers AB, Pardoen JA, Courtin JML, Winkel C, Lugtenburg J, Mathies RA. Vibrational analysis of the all-trans-retinal chromophore in light-adapted bacteriorhodopsin. J Am Chem Soc. 1987; 109:3108–3125.
20. Ogren JI, Mamaev S, Russano D, Li H, Spudich JL, Rothschild KJ. Retinal chromophore structure and Schiff base interactions in red-shifted channelrhodopsin-1 from Chlamydomonas augustae. Biochemistry. 2014; 53:3961–3970. [PubMed: 24869998]
21. Maeda A, Tomson FL, Gennis RB, Balashov SP, Ebrey TG. Water molecule rearrangements around Leu93 and Trp182 in the formation of the L intermediate in bacteriorhodopsin's photocycle. Biochemistry. 2003; 42:2535–2541. [PubMed: 12614147]
22. Gerwert K, Siebert F. Evidence for light-induced 13-cis, 14-s-cis isomerization in bacteriorhodopsin obtained by FTIR difference spectroscopy using isotopically labelled retinals. EMBO J. 1986; 5:805–811. [PubMed: 16453681]
23. Rothschild KJ, Andrew J, DeGrip WJ, Stanley HE. Opsin Structure Probed by Raman Spectroscopy of Photorecptor Membranes. Science. 1976; 191:1176–1178. [PubMed: 1257742]
24. Rothschild KJ, Zagaeski M, Cantore WA. Conformational changes of bacteriorhodopsin detected by Fourier transform infrared difference spectroscopy. Biochem Biophys Res Commun. 1981; 103:483–489. [PubMed: 7332553]
25. Braiman MS, Rothschild KJ. Fourier transform infrared techniques for probing membrane protein structure. Annu Rev Biophys Biophys Chem. 1988; 17:541–570. [PubMed: 3293599]
26. Braiman MS, Mogi T, Marti T, Stern LJ, Khorana HG, Rothschild KJ. Vibrational spectroscopy of bacteriorhodopsin mutants: light-driven proton transport involves protonation changes of aspartic acid residues 85, 96, and 212. Biochemistry. 1988; 27:8516–8520. [PubMed: 2851326]
27. Roepe P, Scherrer P, Ahl PL, Das Gupta SK, Bogomolni RA, Herzfeld J, Rothschild KJ. Tyrosine and carboxyl protonation changes in the bacteriorhodopsin photocycle. 2. Tyrosines-26 and –64. Biochemistry. 1987; 26:6708–6717. [PubMed: 3427039]

28. Roepe P, Ahl PL, Das Gupta SK, Herzfeld J, Rothschild KJ. Tyrosine and carboxyl protonation changes in the bacteriorhodopsin photocycle. 1. M412 and L550 intermediates. Biochemistry. 1987; 26:6696–6707. [PubMed: 3427038]
29. Kato HE, Zhang F, Yizhar O, Ramakrishnan C, Nishizawa T, Hirata K, Ito J, Aita Y, Tsukazaki T, Hayashi S, Hegemann P, Maturana AD, Ishitani R, Deisseroth K, Nureki O. Crystal structure of the channelrhodopsin light-gated cation channel. Nature. 2012; 482:369–374. [PubMed: 22266941]
30. Amsden JJ, Kralj JM, Bergo VB, Spudich EN, Spudich JL, Rothschild KJ. Different structural changes occur in blue- and green-proteorhodopsins during the primary photoreaction. Biochemistry. 2008; 47:11490–11498. [PubMed: 18842006]
31. Marrero H, Rothschild KJ. Bacteriorhodopsin's M412 and Br605 protein conformations are similar. FEBS Lett. 1987; 223:289–293.
32. Nack M, Radu I, Bamann C, Bamberg E, Heberle J. The retinal structure of channelrhodopsin-2 assessed by resonance Raman spectroscopy. FEBS Lett. 2009; 583:3676–3680. [PubMed: 19854176]
33. Bruun S, Stoeppler D, Keidel A, Kuhlmann U, Luck M, Diehl A, Geiger MA, Woodmansee D, Trauner D, Hegemann P, Oschkinat H, Hildebrandt P, Stehfest K. Light-Dark Adaptation of Channelrhodopsin Involves Photoconversion between the all-trans and 13-cis Retinal Isomers. Biochemistry. 2015; 54:5389–5400. [PubMed: 26237332]
34. Govorunova EG, Sineshchekov OA, Rodarte EM, Janz R, Morelle O, Melkonian M, Wong GK, Spudich JL. The Expanding Family of Natural Anion Channelrhodopsins Reveals Large Variations in Kinetics, Conductance, and Spectral Sensitivity. Sci Rep. 2017; 7:43358. [PubMed: 28256618]
35. Siebert F, Mäntele W. Investigation of the primary photochemistry of bacteriorhodopsin by low-temperature Fourier-transform infrared spectroscopy. Eur J Biochem. 1983; 130:565–573. [PubMed: 6825710]
36. Rothschild KJ, Marrero H, Braiman M, Mathies R. Primary photochemistry of bacteriorhodopsin: comparison of Fourier transform infrared difference spectra with resonance Raman spectra. Photochem Photobiol. 1984; 40:675–679. [PubMed: 6514815]
37. de Groot HJM, Smith SO, Courtin J, Van den Berg E, Winkel C, Lugtenburg J, Griffin RG, Herzfeld J. Solid-state carbon-13 and nitrogen-15 NMR study of the low pH forms of bacteriorhodopsin. Biochemistry. 1990; 29:6873–6883. [PubMed: 2168744]
38. Maeda A, Sasaki J, Shichida Y, Yoshizawa T, Chang M, Ni B, Needleman R, Lanyi JK. Structures of aspartic acid-96 in the L and N intermediates of bacteriorhodopsin: analysis by Fourier transform infrared spectroscopy. Biochemistry. 1992; 31:4684–4690. [PubMed: 1316157]
39. Rothschild KJ. The early development and application of FTIR difference spectroscopy to membrane proteins: A personal perspective. Biomed Spectrosc Imaging. 2016; 5:231–267.
40. Balashov SP, Ebrey TG. Trapping and spectroscopic identification of the photointermediates of bacteriorhodopsin at low temperatures. Photochem Photobiol. 2001; 73:453–462. [PubMed: 11367564]
41. Edmonds BW, Luecke H. Atomic resolution structures and the mechanism of ion pumping in bacteriorhodopsin. Front Biosci, Landmark Ed. 2004; 9:1556–1566.
42. Gerwert K, Souvignier G, Hess B. Simultaneous monitoring of light-induced changes in protein side-group protonation, chromophore isomerization, and backbone motion of bacteriorhodopsin by time-resolved Fourier-transform infrared spectroscopy. Proc Natl Acad Sci U S A. 1990; 87:9774–9778. [PubMed: 11607137]
43. Lorenz-Fonfria VA, Muders V, Schlesinger R, Heberle J. Changes in the hydrogen-bonding strength of internal water molecules and cysteine residues in the conductive state of channelrhodopsin-1. J Chem Phys. 2014; 141:22D507.
44. Kuhne J, Eisenhauer K, Ritter E, Hegemann P, Gerwert K, Bartl F. Early formation of the ion-conducting pore in channelrhodopsin-2. Angew Chem, Int Ed. 2015; 54:4953–4957.
45. Wietek J, Wiegert JS, Adeishvili N, Schneider F, Watanabe H, Tsunoda SP, Vogt A, Elstner M, Oertner TG, Hegemann P. Conversion of channelrhodopsin into a light-gated chloride channel. Science. 2014; 344:409–412. [PubMed: 24674867]

46. Muders V, Kerruth S, Lorenz-Fonfria VA, Bamann C, Heberle J, Schlesinger R. Resonance Raman and FTIR spectroscopic characterization of the closed and open states of channelrhodopsin-1. FEBS Lett. 2014; 588:2301–2306. [PubMed: 24859039]
47. Ritter E, Piwowarski P, Hegemann P, Bartl FJ. Light-dark adaptation of channelrhodopsin C128T mutant. J Biol Chem. 2013; 288:10451–10458. [PubMed: 23439646]
48. Neumann-Verhoefen MK, Neumann K, Bamann C, Radu I, Heberle J, Bamberg E, Wachtveitl J. Ultrafast infrared spectroscopy on channelrhodopsin-2 reveals efficient energy transfer from the retinal chromophore to the protein. J Am Chem Soc. 2013; 135:6968–6976. [PubMed: 23537405]
49. Lorenz-Fonfria VA, Resler T, Krause N, Nack M, Gossing M, Fischer von Mollard G, Bamann C, Bamberg E, Schlesinger R, Heberle J. Transient protonation changes in channelrhodopsin-2 and their relevance to channel gating. Proc Natl Acad Sci U S A. 2013; 110:E1273–1281. [PubMed: 23509282]
50. Braiman M, Mathies R. Resonance Raman spectra of bacteriorhodopsin's primary photoproduct: evidence for a distorted 13-cis retinal chromophore. Proc Natl Acad Sci U S A. 1982; 79:403–407. [PubMed: 6281770]
51. Argade PV, Rothschild KJ. Quantitative Analysis of Resonance Raman Spectra of Purple Membrane from *Halobacterium halobium*: L550 intermediate. Biochemistry. 1983; 22:3460–3466.
52. Fodor SPA, Pollard WT, Gebhard R, Van den Berg EMM, Lugtenburg J, Mathies RA. Bacteriorhodopsin's L550 intermediate contains a C14–C15 s-trans-retinal chromophore. Proc Natl Acad Sci U S A. 1988; 85:2156–2160. [PubMed: 3353373]
53. Tanimoto T, Furutani Y, Kandori H. Structural changes of water in the Schiff base region of bacteriorhodopsin: proposal of a hydration switch model. Biochemistry. 2003; 42:2300–2306. [PubMed: 12600197]
54. Rothschild KJ, Marrero H. Infrared evidence that the Schiff base of bacteriorhodopsin is protonated: bR570 and K intermediates. Proc Natl Acad Sci U S A. 1982; 79:4045–4049. [PubMed: 6955790]
55. Kitajima-Ihara T, Furutani Y, Suzuki D, Ihara K, Kandori H, Homma M, Sudo Y. Salinibacter sensory rhodopsin: sensory rhodopsin I-like protein from a eubacterium. J Biol Chem. 2008; 283:23533–23541. [PubMed: 18566451]
56. Suzuki D, Sudo Y, Furutani Y, Takahashi H, Homma M, Kandori H. Structural changes of Salinibacter sensory rhodopsin I upon formation of the K and M photointermediates. Biochemistry. 2008; 47:12750–12759. [PubMed: 18991393]
57. Bergo VB, Ntefidou M, Trivedi VD, Amsden JJ, Kralj JM, Rothschild KJ, Spudich JL. Conformational changes in the photocycle of Anabaena sensory rhodopsin: absence of the Schiff base counterion protonation signal. J Biol Chem. 2006; 281:15208–15214. [PubMed: 16537532]
58. Verhoefen MK, Schafer G, Shastri S, Weber I, Glaubitz C, Mäntele W, Wachtveitl J. Low temperature FTIR spectroscopy provides new insights in the pH-dependent proton pathway of proteorhodopsin. Biochim Biophys Acta, Bioenerg. 2011; 1807:1583–1590.
59. Amsden JJ, Kralj JM, Chieffo LR, Wang X, Erramilli S, Spudich EN, Spudich JL, Ziegler LD, Rothschild KJ. Subpicosecond protein backbone changes detected during the green-absorbing proteorhodopsin primary photoreaction. J Phys Chem B. 2007; 111:11824–11831. [PubMed: 17880126]
60. Kralj JM, Bergo VB, Amsden JJ, Spudich EN, Spudich JL, Rothschild KJ. Protonation state of Glu142 differs in the green- and blue-absorbing variants of proteorhodopsin. Biochemistry. 2008; 47:3447–3453. [PubMed: 18284210]
61. Kralj JM, Spudich EN, Spudich JL, Rothschild KJ. Raman spectroscopy reveals direct chromophore interactions in the Leu/Gln105 spectral tuning switch of proteorhodopsins. J Phys Chem B. 2008; 112:11770–11776. [PubMed: 18717545]
62. Bergo VB, Sineshchekov OA, Kralj JM, Partha R, Spudich EN, Rothschild KJ, Spudich JL. His-75 in proteorhodopsin, a novel component in light-driven proton trans-location by primary pumps. J Biol Chem. 2009; 284:2836–2843. [PubMed: 19015272]
63. Bayraktar H, Fields AP, Kralj JM, Spudich JL, Rothschild KJ, Cohen AE. Ultrasensitive measurements of microbial rhodopsin photocycles using photochromic FRET. Photochem Photobiol. 2012; 88:90–97. [PubMed: 22010969]

64. Clair EC, Ogren JI, Mamaev S, Kralj JM, Rothschild KJ. Conformational changes in the archaerhodopsin-3 proton pump: detection of conserved strongly hydrogen bonded water networks. J Biol Phys. 2012; 38:153–168. [PubMed: 23277676]

65. Saint Clair EC, Ogren JI, Mamaev S, Russano D, Kralj JM, Rothschild KJ. Near-IR resonance Raman spectroscopy of archaerhodopsin 3: effects of transmembrane potential. J Phys Chem B. 2012; 116:14592–14601. [PubMed: 23189985]

66. Rothschild KJ, Cantore WA, Marrero H. Fourier transform infrared difference spectra of intermediates in rhodopsin bleaching. Science. 1983; 219:1333–1335. [PubMed: 6828860]

67. Tajkhorshid E, Baudry J, Schulten K, Suhai S. Molecular dynamics study of the nature and origin of retinal's twisted structure in bacteriorhodopsin. Biophys J. 2000; 78:683–693. [PubMed: 10653781]

68. Hiraki K, Hamanaka T, Zheng XG, Shinada T, Kim JM, Yoshihara K, Kito Y. Bacteriorhodopsin analog regenerated with 13-desmethyl-13-iodoretinal. Biophys J. 2002; 83:3460–3469. [PubMed: 12496112]

69. Hirai T, Subramaniam S. Protein conformational changes in the bacteriorhodopsin photocycle: comparison of findings from electron and X-ray crystallographic analyses. PLoS One. 2009; 4:e5769. [PubMed: 19488399]

70. Govorunova EG, Sineshchekov OA, Li H, Spudich JL. Microbial rhodopsins: Diversity, mechanisms, and optogenetic applications. Annu Rev Biochem. 2017 n/a.

71. Richards FM. Areas, volumes, packing and protein structure. Annu Rev Biophys Bioeng. 1977; 6:151–176. [PubMed: 326146]

72. Beja O, Aravind L, Koonin EV, Suzuki MT, Hadd A, Nguyen LP, Jovanovich SB, Gates CM, Feldman RA, Spudich JL, Spudich EN, DeLong EF. Bacterial rhodopsin: evidence for a new type of phototrophy in the sea. Science. 2000; 289:1902–1906. [PubMed: 10988064]

73. Beja O, Spudich EN, Spudich JL, Leclerc M, DeLong EF. Proteorhodopsin phototrophy in the ocean. Nature. 2001; 411:786–789. [PubMed: 11459054]

74. Man D, Wang W, Sabehi G, Aravind L, Post AF, Massana R, Spudich EN, Spudich JL, Beja O. Diversification and spectral tuning in marine proteorhodopsins. EMBO J. 2003; 22:1725–1731. [PubMed: 12682005]

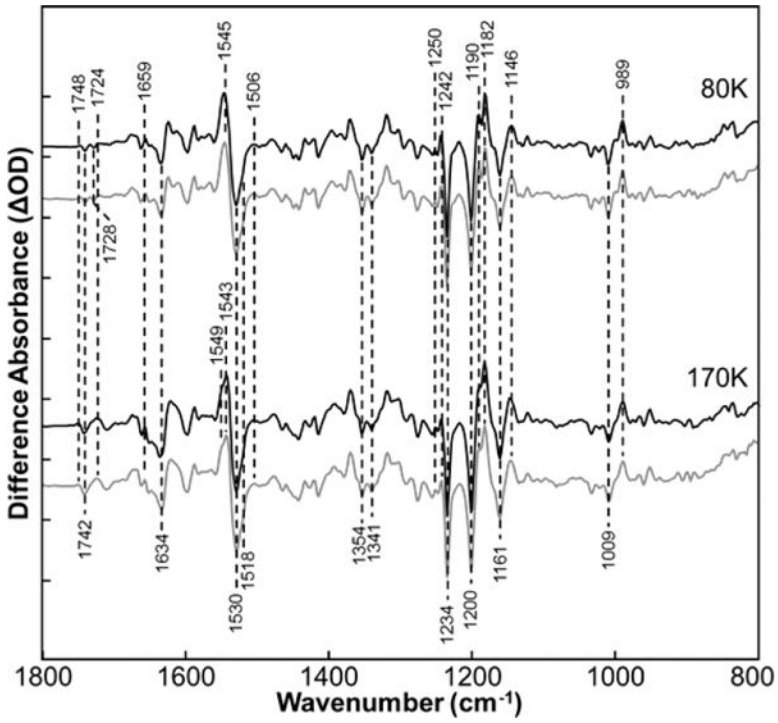


**Figure 1.**

Comparison of first-push FTIR difference spectra (see Materials and Methods) for *Gt*ACR1 recorded at 80 and 170 K. Black lines and gray lines are the result of two independent experiments. Spectra are scaled using the negative peak near 1234 $cm^{-1}$. The *Y*-axis tick mark spacing corresponds to approximately 1.5 mOD for 80 K spectra and 1 mOD for 170 K spectra.

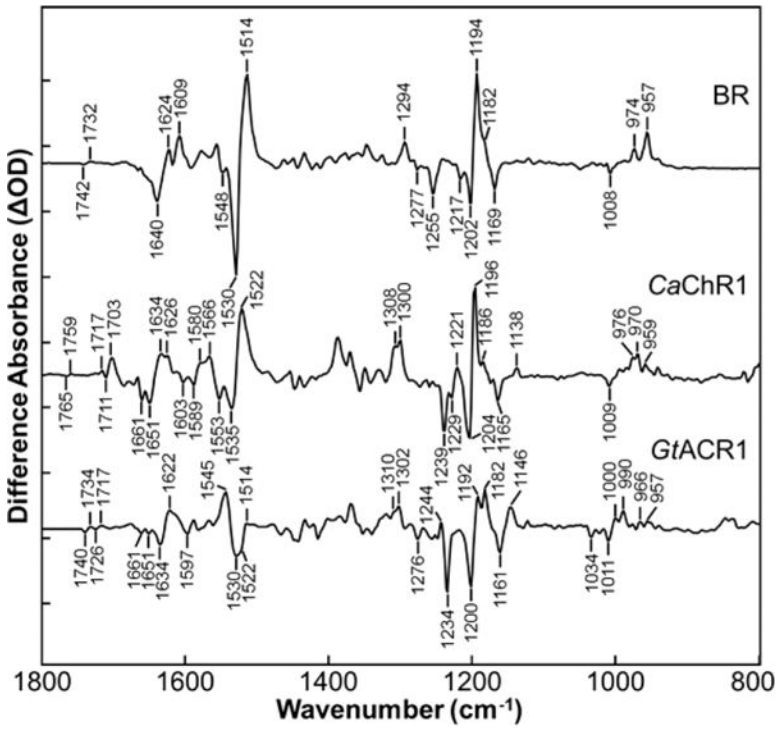


**Figure 2.**

Comparison of averaged photoreversal FTIR difference spectra (see Materials and Methods) for BR, *Ca*ChR1, and *Gt*ACR1 recorded at 80 K. The *Y*-axis tick mark spacing corresponds to approximately 5 mOD for BR and 1 mOD for *Ca*ChR1 and *Gt*ACR1. Each difference spectrum consisted of average of at least 30 spectra.

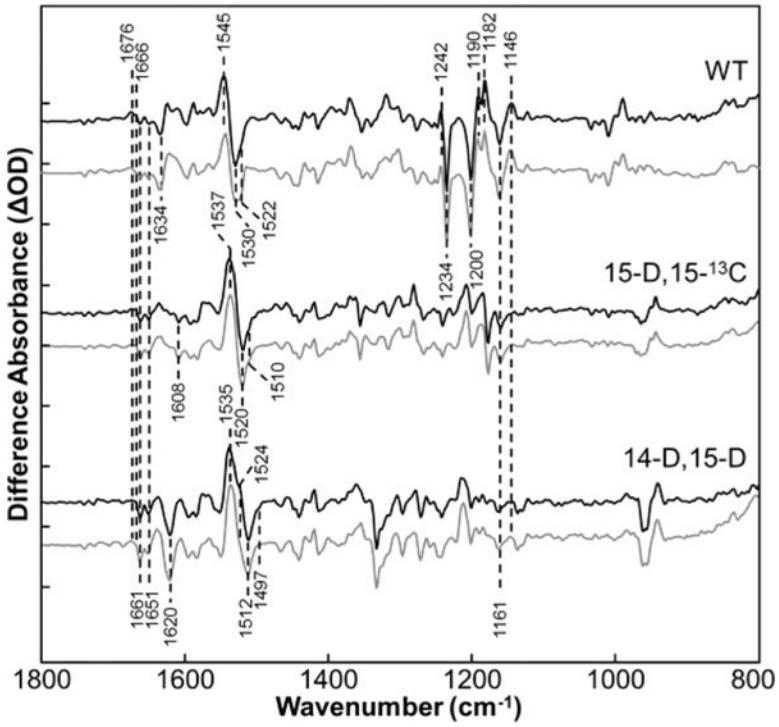


**Figure 3.**

Comparison of first-push FTIR difference spectra at 80 K for *Gt*ACR1 WT sample and samples regenerated using [15-D,15-$^{13}$C]- and [14-D,15D]retinals as described in Materials and Methods. Black lines are spectra from single-push experiments using 530 nm illumination, and gray lines are averaged spectra (see Materials and Methods). Spectra are scaled such that the positive and negative peaks in the 1510–1550 cm$^{-1}$ regions are similar in size. The *Y*-axis tick mark spacing corresponds to approximately 1.5, 1, 1, 0.5, 1, and 0.5 mOD from top to bottom, respectively.

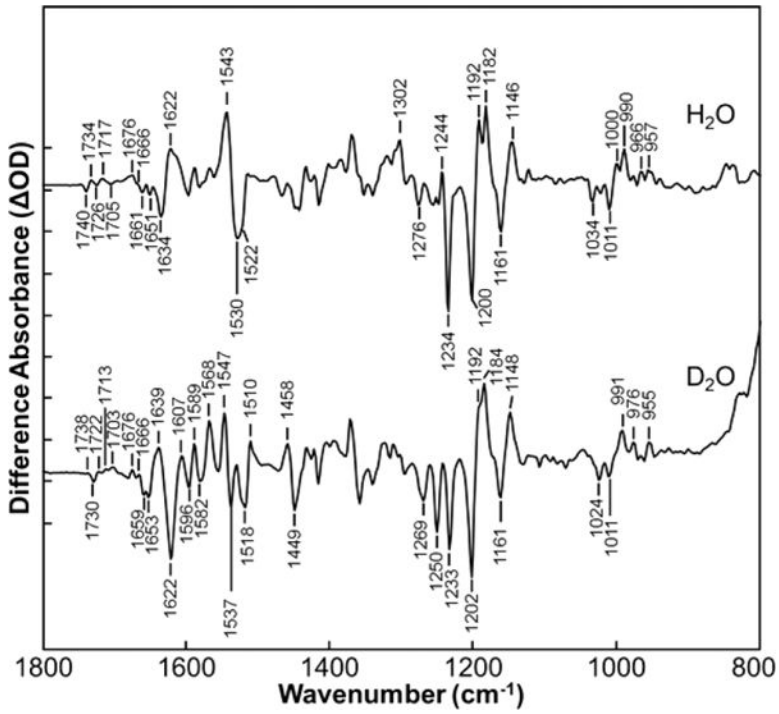


**Figure 4.**

Comparison of first-push FTIR difference spectra for *Gt*ACR1 in $H_2O$ and $D_2O$ recorded at 80 K. Spectra are scaled using the negative peak near 1200 $cm^{-1}$. The *Y*-axis tick mark spacing corresponds to approximately 0.5 mOD for the $H_2O$ spectrum and 0.1 mOD for the $D_2O$ spectrum.

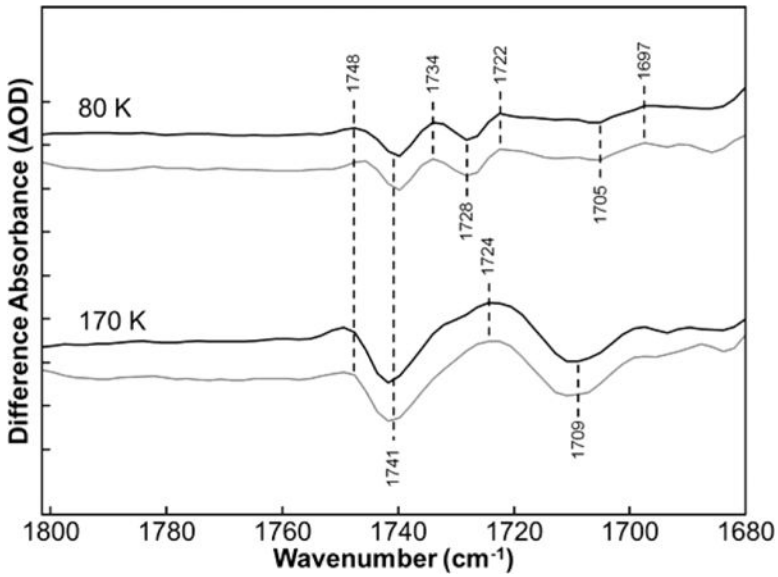


**Figure 5.**

Comparison of first-push FTIR difference spectra for *Gt*ACR1 recorded at 80 and 170 K over the 1680–1800 $cm^{-1}$ region. Spectra are scaled using the negative peak near 1234 $cm^{-1}$. Black lines and gray lines are results from two independent experiments. The *Y*-axis tick mark spacing corresponds to approximately 0.15 mOD for 80 K spectra and 0.1 mOD for 170 K spectra.

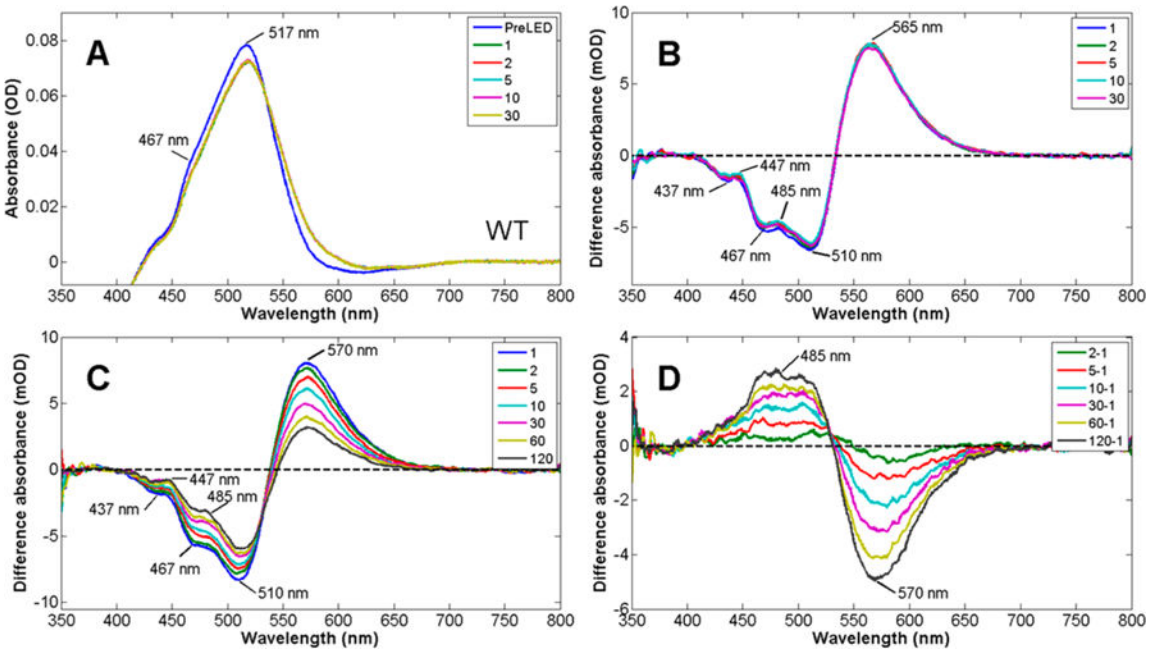


**Figure 6.**

(A) Low-temperature UV–visible baseline-corrected spectra of *Gt*ACR1 recorded at 80 K before and various times after illumination. (B) UV–visible difference spectra computed from spectra in panel A (differences consist of subtraction of postspectra from the prespectrum) using baseline correction. (C) Same as panel B but spectra recorded at 170 K. (D) Difference of difference spectra shown in panel C computed by subtracting the first difference spectrum from subsequent difference spectra. All legends for figures are in minutes.

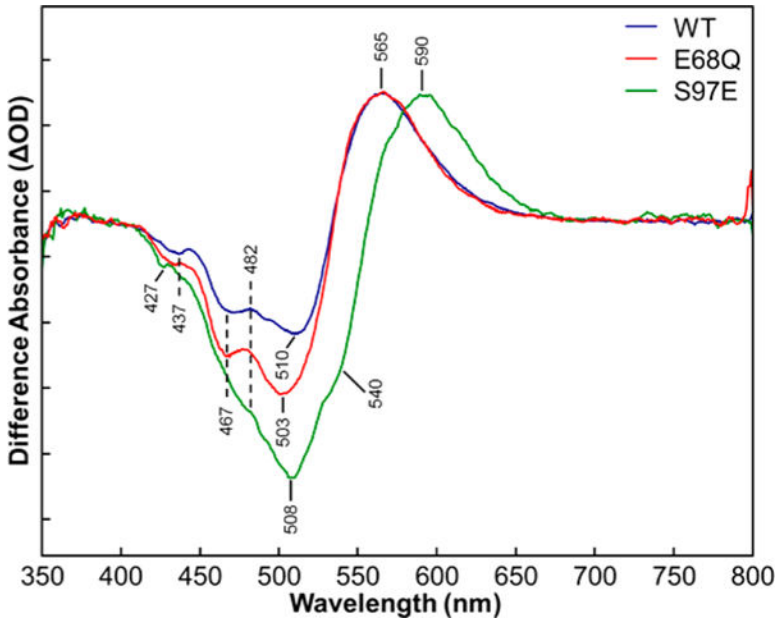


**Figure 7.**

Comparison of UV–vis difference spectra of *Gt*ACR1 WT (blue) and its mutants E68Q (red) and S97E (green) recorded at 80 K. Spectra were baseline-corrected as described in Methods and Materials and scaled using the positive peak near 656 nm (WT and E68Q) and 592 nm (S97E). The *Y*-axis tick mark spacing corresponds to approximately 4 mOD for WT and 2 mOD for the two mutants.

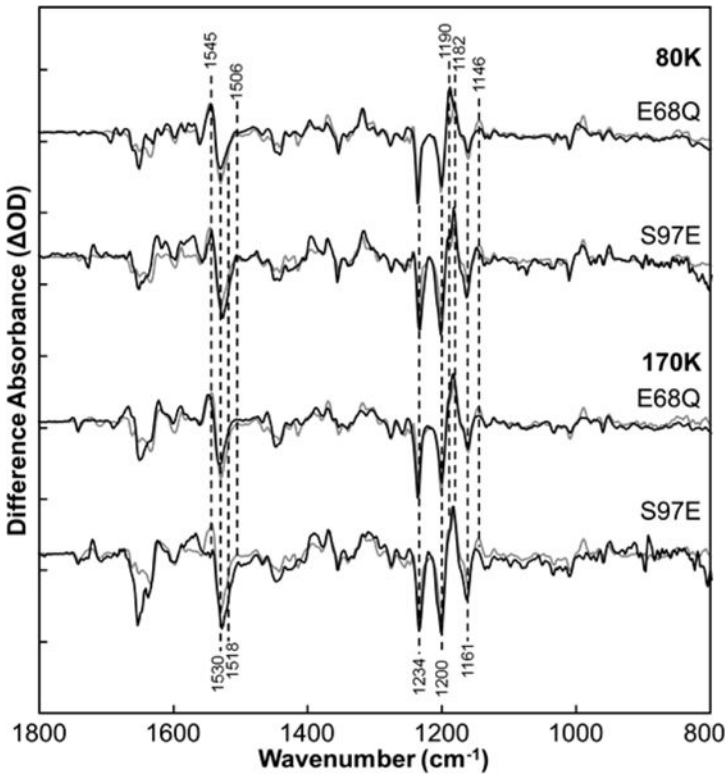


**Figure 8.**

Comparison of first-push "3–1" (see Materials and Methods) FTIR difference spectra for *Gt*ACR1 with its mutants E68Q and S97E recorded at 80 and 170 K. Gray lines are wild-type spectra, and black lines are E68Q or S97E spectra. Spectra are scaled using the negative peak near 1234 $cm^{-1}$. The *Y*-axis tick mark spacing corresponds to approximately 2 mOD for WT at 80 K, 1.5 mOD for WT at 170 K, 1.5 mOD for E68Q at both temperatures, and 0.5 mOD for S97E at both temperatures.

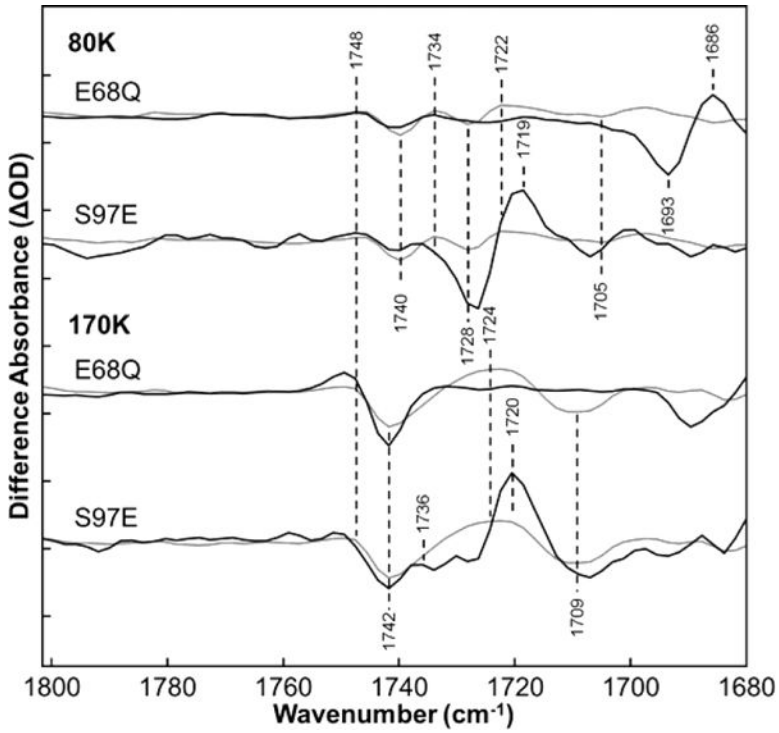


**Figure 9.**

Comparison of first-push 3–1 (see Materials and Methods) FTIR difference spectra for *Gt*ACR1 with its mutants E68Q and S97E recorded at 80 and 170 K over the 1680–1800 $cm^{-1}$ region. Gray lines are wild-type spectra, and black lines are E68Q or S97E spectra as indicated. Spectra are scaled using the negative peak near 1234 $cm^{-1}$. The *Y*-axis tick mark spacing corresponds to approximately 0.4 mOD for WT at 80 K, 0.3 mOD for WT at 170 K, 0.3 mOD for E68Q at both temperatures, and 0.1 mOD for S97E at both temperatures.

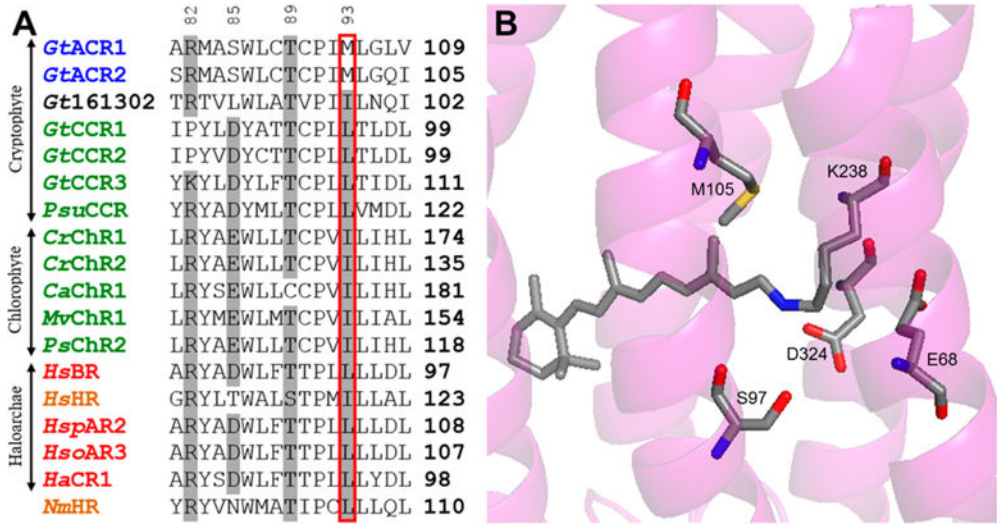


**Figure 10.**

Alignments of transmembrane helix 3 for various microbial rhodopsins. Microbial rhodopsins listed are color-coded with blue representing anion channelrhodopsins (ACRs), green representing cation channelrhodopsins (CCRs), red representing proton ($H^+$) pumps, and orange representing chloride ($Cl^-$) pumps. Residues homologous to BR Leu93 are shown with a red border. The top numbering is from the BR sequence, and numbers to the right show the last residue in the sequence for each microbial rhodopsin listed. The proteins are further divided as indicated by arrows into classifications of cryptophyte algae, chlorophyte algae, and haloarchae (see the arrow). Abbreviations: *Gt*, *G. theta*; *Psu*, *Proteomonas sulcata*; *Cr*, *C. reinhardtii*; *Ca*, *C. augustae*; *Mv*, *Mesostigma viride*; *Ps*, *Platymonas subcordiformis*; *Hs*, *Halobacterium salinarum*; *Hsp*, *Halobacterium* sp. aus-2; *Hso*, *Halorubrum sodomense*; *Ha*, *Haloarcula argentinos*. Note that *Nanolabens marimus* is a flavobacterium. (B) Three-dimensional structure of the C1–C2 chimera from ref [29] (Protein Data Bank entry 3UG9) with selected residues from *Gt*ACR1 substituted (E68, S97, M105, D234, and K238) instead of C1–C2 residues (E129, E162, I170, D292, and K296). The numbering is based on the *Gt*ACR1 sequence.